Magnetic phase boundary of BaVS3 clarified with high-pressure mu+SR

(article starts on next page)

Magnetic phase boundary of BaVS$_3$ clarified with high-pressure μ^+SR

Jun Sugiyama [©],[1,2,3,*] Daniel Andreica,[4] Ola Kenji Forslund [©],[5] Elisabetta Nocerino,[5] Nami Matsubara [©],[5] Yasmine Sassa,[6] Zurab Guguchia,[7] Rustem Khasanov,[7] Francis L. Pratt,[8] Hiroyuki Nakamura [©],[9] and Martin Månsson [©][5]

[1]*CROSS Neutron Science and Technology Center, Tokai, Ibaraki 319-1106, Japan*
[2]*Advanced Science Research Center, Japan Atomic Energy Agency, Tokai, Ibaraki 319-1195, Japan*
[3]*High Energy Accelerator Research Organization (KEK), Tokai, Ibaraki 319-1106, Japan*
[4]*Faculty of Physics, Babes-Bolyai University, 400084, Cluj-Napoca, Romania*
[5]*Department of Applied Physics, KTH Royal Institute of Technology, Electrum 229, SE-16440, Stockholm, Kista, Sweden*
[6]*Department of Physics, Chalmers University of Technology, SE-412 96 Göteborg Sweden*
[7]*Laboratory for Muon Spin Spectroscopy, Paul Scherrer Institute, CH-5232, Villigen, PSI, Switzerland*
[8]*ISIS Pulsed Neutron and Muon Facility, STFC Rutherford Appleton Laboratory, Harwell Oxford, Didcot OX11 OQX, United Kingdom*
[9]*Department of Materials Science and Engineering, Kyoto University, Kyoto 606-8501, Japan*

The magnetic nature of the quasi-one-dimensional BaVS$_3$ has been studied as a function of temperature down to 0.25 K and pressure up to 1.97 GPa on a powder sample using the positive muon spin rotation and relaxation (μ^+SR) technique. At ambient pressure, BaVS$_3$ enters an incommensurate antiferromagnetic ordered state below the Néel temperature (T_N) 31 K. T_N is almost constant as the pressure (p) increases from ambient pressure to 1.4 GPa, then T_N decreases rapidly for $p > 1.4$ GPa, and finally disappears at $p \sim 1.8$ GPa, above which a metallic phase is stabilized. Hence, T_N is found to be equivalent to the pressure-induced metal-insulator transition temperature (T_{MI}) at $p > 1.4$ GPa.

I. INTRODUCTION

The magnetic ground state of the two-dimensional triangular lattice with $S = \frac{1}{2}$ is expected to vary with the external pressure (p), mainly due to a change in the interactions between the nearest-neighboring magnetic ions [1]. Particularly for the quasi-one-dimensional (Q1D) compound BaVS$_3$ (see Fig. 1) [2–6], in which the 1D ferromagnetic (FM) interaction along the c axis is stronger than the two-dimensional (2D) antiferromagnetic (AF) interaction along the a axis [7], a metal-insulator transition occurs at $T_{MI} = 70$ K at ambient pressure. However, as p increases, T_{MI} is found to vanish at a critical pressure (p_{cr}) ~ 1.8 GPa, based on resistivity, infrared, and x-ray diffraction (XRD) measurements [8–11]. The metal-insulator transition is thought to be induced by the formation of a commensurate charge-density wave (CDW) Peierls ground state below T_{MI} with the doubling of the c-axis length. Interestingly, such second-order Peierls transition disappears at $p \sim 1.5$ GPa, and a commensurate-incommensurate (C-IC) first-order structural transition occurs instead. Finally, a metallic ground state is stabilized at $p \geqslant 1.8$ GPa, implying the presence of a quantum critical transition (QCT) in BaVS$_3$ [12].

Despite the drastic changes in structural and electrical properties at T_{MI} mentioned above, a magnetic transition is found to occur at 30 K and not at T_{MI}. That is, even though the magnetization-vs-temperature [$M(T)$] curve exhibits a sharp

maximum at T_{MI} [3–5], past NMR [14,15] and neutron diffraction work [16] clarified that BaVS$_3$ undergoes a magnetic transition from a high-T paramagnetic state to a low-T IC-AF ordered state below $T_N = 30$ K at ambient pressure. The IC magnetic modulation vector was assigned to (0.226 0.226 0) in a hexagonal setting and the ordered magnetic moment was estimated as $\sim 0.5 \mu_B$ at 4 K [16]. The details of the IC-AF state are still unknown, but either a linear or a cycloidal spin density wave (SDW) order state was proposed as a ground state. In addition, since at present there is no available data on the pressure dependence of T_N, the following three scenarios were proposed for the $T - p$ phase diagram of BaVS$_3$ [17]:

(1) T_N is suppressed to zero at $p < p_{cr}$,
(2) T_N is suppressed to zero at $p = p_{cr}$, or
(3) T_N is suppressed to zero at $p > p_{cr}$.

Based on magnetoresistance measurements under high pressures, scenario 3 was thought to be suitable for BaVS$_3$ [17,18]. Note that, besides scenario 2, the IC-AF order is assumed to be independent of the structural modification caused by the CDW formation. Such independence is consistent with the fact that $T_{MI} = 70$ K, whereas $T_N = 30$ K at ambient pressure.

To understand the correlation between the crystal structure and the magnetic order, an essential first step would be to clarify the pressure dependence of T_N in BaVS$_3$ with direct magnetic measurements. A positive muon spin rotation and relaxation (μ^+SR) experiment has therefore been performed under pressures up to 2 GPa. The μ^+SR technique is one of the most powerful tools for studying internal magnetic fields in solids [19,20] including the Q1D compounds [21–24], and,

*juns@triumf.ca or j_sugiyama@cross.or.jp

in this paper, it demonstrates that scenario 2 is realized in $BaVS_3$.

II. EXPERIMENTAL

A powder sample of $BaVS_3$ was prepared by a conventional solid-state-reaction technique reported in Ref. [5]. That is, a mixture of BaS (99.9%+), V (99.9%), and S (99.9999%) was heated in an evacuated quartz tube at 1223 K for four days. The reaction mixture was ground and then heated at 923 K with excess sulfur in an evacuated quartz tube for three days to avoid sulfur deficiency. After the synthesis, the powdered sample was characterized by XRD. Later, the sample was sealed in a quartz tube together with S and transferred to the Paul Sherrer Institute (PSI) in Switzerland. Immediately before the μ^+SR measurements, the sample was removed from the quartz tube.

The μ^+SR spectra of $BaVS_3$ were recorded using both the General Purpose Spectrometer (GPS) at the surface muon beam-line piM3 and the General Purpose Decay-Channel Spectrometer (GPD) at the decay beam line muE4 of the Laboratory for muon spin spectroscopy (LMU) of the PSI in Switzerland. On the GPS, approximately 200 mg of powder sample was placed in an envelope with $1 \times 1 \, cm^2$ area, made of Al-coated Mylar tape with 0.05 mm thickness to minimize the signal from the envelope. The envelope was attached to a fork-type low-background sample holder and inserted in a liquid-He flow-type cryostat for measurements in a temperature range between 2 and 40 K.

On the GPD, three pelletized discs of the powder sample with 6-mm diameter and 15-mm total height (5 mm each) were stacked in a piston-cylinder-type pressure cell made of MP35 alloy. To apply hydrostatic pressure to the sample, Daphne oil was used as a pressure-transmitting medium. The actual pressure at low temperatures was estimated by measuring the superconducting transition temperature of an indium wire placed at the bottom of the sample space, by AC susceptibility. The accuracy of the pressure determined by such measurement is estimated as ± 0.01 GPa [25]. A Janis ^{4}He flow cryostat and a Quantum ^{4}He cryostat with a ^{3}He insert were used to reach temperatures as low as 2 K and 0.25 K, respectively.

The experimental techniques are described in more detail elsewhere [19,20,26,27]. The obtained μ^+SR data was analyzed with the MUSRFIT software suite [28].

The muon sites in the $BaVS_3$ lattice were predicted by density-functional theory (DFT) calculations for the total electron energy with the VASP code package [29]. Such predictions reveal that there are two possible muon sites in the lattice. That is, (2/3, 1/3, 3/4) and (1/3, 1/3, 1/2) (see Fig. 1).

III. RESULTS AND DISCUSSION

In this section, the microscopic magnetic nature of $BaVS_3$ under ambient pressure is described in the first two subsections (Secs. III A and III B). Pressure-dependent results, the main part of this paper, are reported in the last two subsections (Secs. III C and III D).
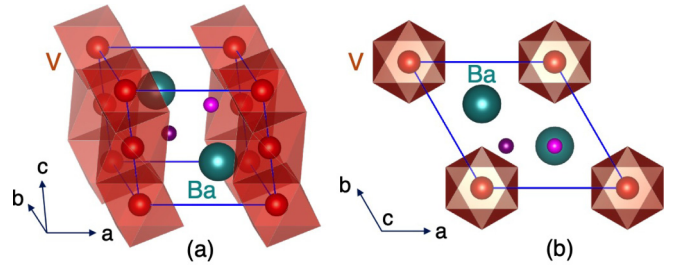

FIG. 1. Crystal structure of hexagonal $BaVS_3$ with space group $P6_3/mmc$ [6] drawn with VESTA [13]. Large deep blue spheres represent Ba and orange medium spheres represent V. Each corner of polyhedra is occupied by S. The two possible muon sites in the lattice predicted by DFT calculations are (2/3, 1/3, 3/4), the pink small sphere, and (1/3, 1/3, 1/2), the violet small sphere. (b) In the *ab* plane, V ions form a two-dimensional triangular lattice.

A. ZF-μ^+SR at ambient pressure

The quality of the present sample is evidenced by the plot in Fig. 2(a), which shows the ZF-μ^+SR spectrum recorded at 2 K at the GPS spectrometer. In Fig. 2(a), one can clearly observe the muon spin precession signal due to the presence of static magnetic order, while in past μ^+SR work [32,33]

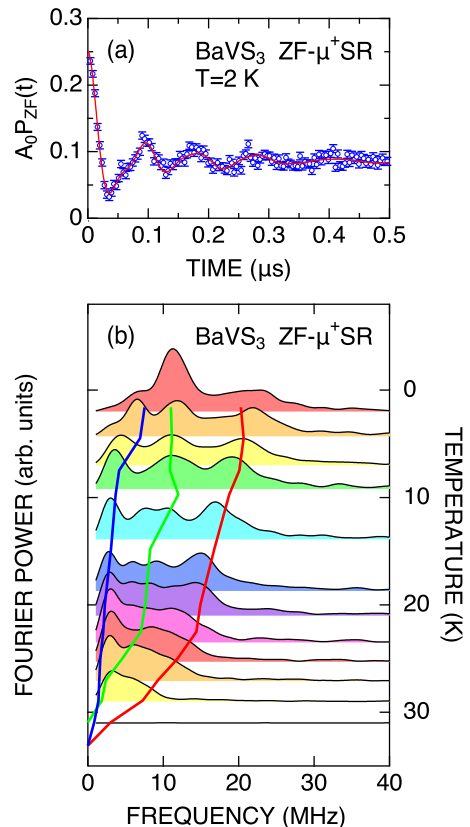FIG. 2. (a) The ZF-μ^+SR time spectrum for $BaVS_3$ recorded at 2 K and (b) the temperature variation of the Fourier transform power frequency spectrum. In (a), a solid line represents a best fit with Eq. (1). In (b), three solid lines represent the muon spin precession frequencies obtained by fitting the ZF-μ^+SR time spectrum with Eq. (1). The data for the three lines are the same as f_{AFi} in Fig. 4(a).
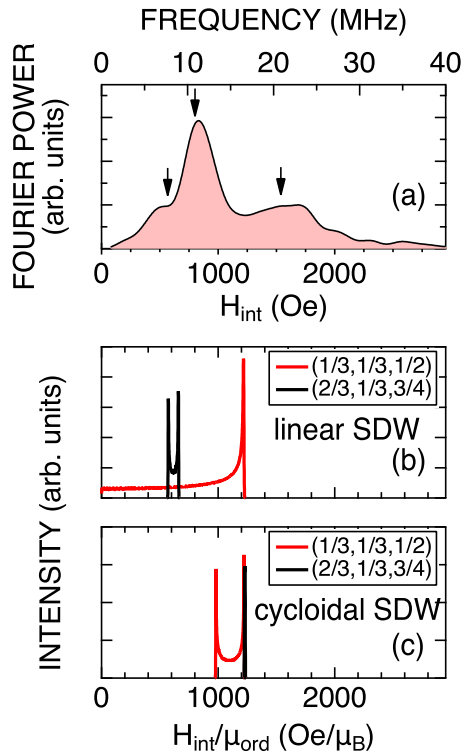
FIG. 3. (a) The Fourier transform power frequency spectrum of BaVS$_3$ obtained from the μ^+SR time spectra recorded at 2 K and the internal magnetic field at the two muon sites predicted by DIPOLE-CALC [30] for (b) the linear IC-SDW order and (c) the cycloidal IC-SDW order with the modulation vector (0.226, 0.226, 0). In (a), arrows show the three frequencies to provide the best fit for the time spectrum in Fig. 2(a) with Eq. (1). Even for the modulation vector (0.226, 0.226, ξ) with $\xi = 0.033$ proposed by resonant magnetic x-ray scattering measurements [31], the filed distributions for both orders are almost the same as those for $\xi = 0$, i.e., (b) and (c). (a) is the same as the top spectrum in Fig. 2(b).

a Kubo-Toyabe-like behavior even at 2 K due to a random internal magnetic field was reported. This is most likely caused by either lower sample quality or sample degradation problems in past work (see Sec. IV).

Since the AF order in BaVS$_3$ is incommensurate to the lattice [16], each muon *feels* a slightly different internal magnetic field. Thus, the ZF-μ^+SR spectrum exhibits a rapidly damped oscillation with multiple frequencies. In fact, the frequency spectrum, i.e., the Fourier transform of the time spectrum, indicates the presence of at least three frequencies, ~ 8 MHz, ~ 11 MHz, and ~ 21 MHz with large field distribution widths [Fig. 3(a)]. The comparison of the measured internal fields with the predicted internal magnetic fields at the two muon sites, i.e., (2/3,1/3,3/4) and (1/3,1/3,1/2), for the linear and the cycloidal IC-SDW order indicates that the linear IC-SDW is most probably realized in BaVS$_3$ below T_N [Figs. 3(b) and 3(c)]. Note that for the linear IC-SDW, the direction of the magnetic moment is fixed and its magnitude is modulated between positive and negative values. For the cycloidal IC-SDW, the propagation vector is in the same *ab* plane as the rotating moments. Furthermore, recent resonant soft XRD measurements suggested the presence of

two magnetically different V ions in the lattice [34], leading to a more complex IC-AF structure than that simulated in Fig. 3. However, at present it is difficult to calculate the internal magnetic field of such IC-AF order due to the absence of data concerning the direction and the magnitude of the ordered magnetic moments of the V ions. Moreover, although μ^+SR sometimes provides essential information to select the most reasonable magnetic structure among multiple proposed candidates [35,36], μ^+SR itself is a local probe and not a suitable tool to identify a magnetic structure, if one is based only on the μ^+SR data. Therefore, precise neutron diffraction experiments using a single-crystal sample is highly required to obtain information on the AF spin structure in BaVS$_3$.

Considering the field distribution shown in Fig. 3(b), the μ^+SR spectrum was fitted by a combination of a Gaussian relaxing Bessel function, contribution from the muons at site (1/3,1/3,1/2); two Gaussian relaxing cosine functions, contribution from the muons at site (2/3,1/3,3/4); an exponentially relaxing nonoscillatory signal for a 1/3 tail signal in a powder sample from the muons at both sites [19,20]; and a time-independent background signal from the muons stopped in nonmagnetic impurity phases in the sample and at surroundings of the sample,

$$
\begin{aligned}
A_0 P_{ZF}(t) = {} & A_{AF1} J_0(2\pi f_{AF1} t) \exp\left(-\frac{\sigma_{AF1}^2 t^2}{2}\right) \\
& + A_{AF2} \cos(2\pi f_{AF2} t + \phi_{AF2}) \exp\left(-\frac{\sigma_{AF2}^2 t^2}{2}\right) \\
& + A_{AF3} \cos(2\pi f_{AF3} t + \phi_{AF3}) \exp\left(-\frac{\sigma_{AF3}^2 t^2}{2}\right) \\
& + A_{tail} \exp(-\lambda_{tail} t) + A_{BG},
\end{aligned} \tag{1}
$$

where A_0 is the initial asymmetry, A_{AF1}, A_{AF2}, A_{AF3}, A_{tail}, and A_{BG} are the asymmetries associated with the five signals, $J_0(2\pi f t)$ is a zeroth-order Bessel function of the first kind that describes the muon polarization evolution in an incommensurate field distribution [19,20,37]. Here, f_{AF1} and f_{AF2} represent higher cutoff frequencies, while f_{AF3} represents a lower cutoff frequency, i.e., $f_{AF1} > f_{AF2} > f_{AF3}$. More precisely, both field distributions for the muons at site (1/3,1/3,1/2) and site (2/3,1/3,3/4) in Fig. 3(b) are characteristic for an IC-AF order. The former single-peak distribution drawn by a red line is well reproduced by J_0, while the latter double-peaked distribution drawn by a black line is better fitted with two cosines than with a combination of J_0 and cosine [37]. This is because J_0 is nonzero even at 0 MHz. The AF3 signal, which corresponds to the lower peak in the double-peaked distribution, is well fitted with a cosine, since such distribution is thought as a delta function in the frequency domain. Furthermore, based on the weak transverse field (wTF) measurements described in Sec. III B, $A_0 = 0.25$, $A_{BG} = 0.025$, and we assume $\sum_{i=1}^{3} A_{AFi} = \frac{2}{3}(A_0 - A_{BG})$ and $A_{tail} = \frac{1}{3}(A_0 - A_{BG})$ at temperatures below 25 K.

Figure 4 shows the temperature dependencies of the μ^+SR parameters in Eq. (1). Each of the three precession frequencies (f_{AFi}) decreases with increasing temperature and disappears at T_N. Below the vicinity of T_N, i.e., at temperatures above 28 K, the AF2 signal merges to the AF3 signal, as seen in
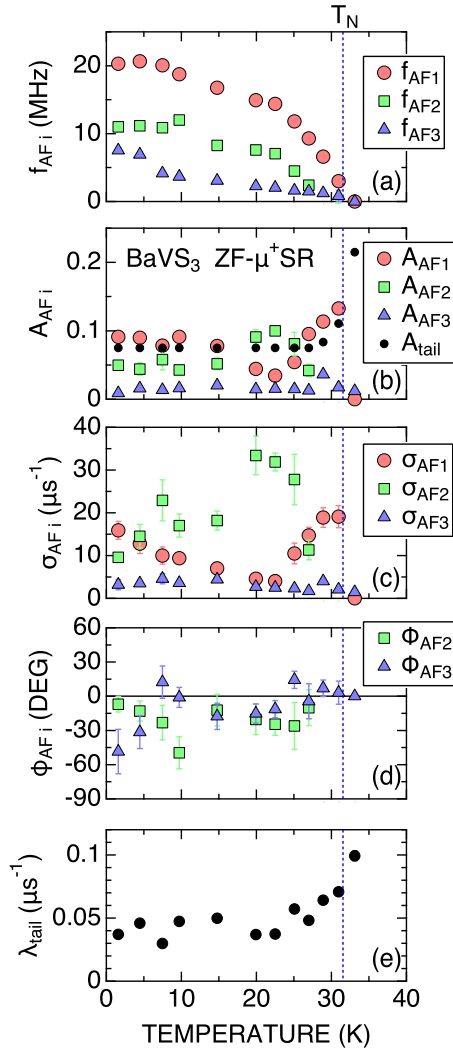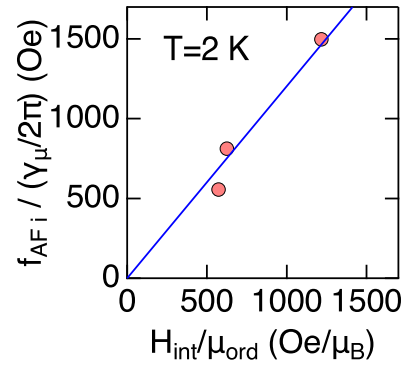
FIG. 5. The relationship between the measured internal magnetic field $[f_{AFi}/(\gamma_\mu/2\pi)]$ at 2 K and the simulated internal magnetic field for the linear SDW. Here, $\gamma_\mu/2\pi$ is the muon gyromagnetic constant (13.554 kHz/Oe). Since the magnetic order is AF, we assumed that the internal magnetic field is equivalent to the dipole field. A solid line represents a linear fit, which provides $\mu_{ord} = 1.20(7)\,\mu_B$ at 2 K. Error bars are smaller than the data point symbol.

FIG. 4. The temperature dependencies of the ZF-μ^+SR parameters in BaVS$_3$ at ambient pressure. (a) The three muon spin precession frequencies (f_{AF1}, f_{AF2}, and f_{AF3}), (b) the normalized asymmetries (A_{AF1}/A_0, A_{AF2}/A_0, A_{AF3}/A_0, and A_{tail}/A_0), (c) the Gaussian relaxation rates of A_{AF} signals (σ_{AF1}, σ_{AF2}, and σ_{AF3}), (d) the delay of the initial phase (ϕ_{AF2} and ϕ_{AF3}), and (e) the exponential relaxation rate of the tail signal (λ_{tail}). The data were obtained by fitting the ZF-μ^+SR spectrum with Eq. (1). Vertical broken lines show the Néel temperature determined by weak transverse field measurements (see Fig. 6); that is, $T_N = 31.55(6)$ K. In (a) and (b), error bars are smaller than the data point symbols.

Fig. 2(b). Using the fitted values of f_{AF1}, f_{AF2}, and f_{AF3} at 2 K and the linear IC-SDW model, the ordered V moment (μ_{ord}^V) is estimated as $1.20(7)\,\mu_B$ (Fig. 5). However, the past neutron work using a powder sample reported that $\mu_{ord}^V \sim 0.5\,\mu_B$ at 4 K, under the assumption that the ordering occurred with a constant magnitude within the *ab* plane [16]. This could be a reason for the underestimation of μ_{ord}^V with neutron diffraction. To clarify the reason for such discrepancy between μ_{ord}^V estimated with μ^+SR and that with neutron diffraction, it is highly preferable to perform neutron diffraction experiments using a high-quality single crystal sample. In fact, for Nd$_2$Fe$_{14}$B magnets, the neutron work using a powder sample reported

that the ordered Nd moment (μ_{ord}^{Nd}) is $\leqslant 1\,\mu_B$ [38] or $1.5\,\mu_B$ [39], while the neutron study using a single-crystal sample revealed that $\mu_{ord}^{Nd} = 3.2\,\mu_B$ [40]. On the contrary, μ^+SR on a powder sample showed that $\mu_{ord}^{Nd} = 3.31\,\mu_B$ [41].

Back to Fig. 4(b), as temperature increases from 2 K, each asymmetry is roughly temperature independent up to around 15 K. Then A_{AF2} increases up to ~ 0.1 at around 22 K, instead of the decreases in A_{AF1}. Then, A_{AF2} decreases with further increasing temperature and merges into A_{AF3} at ~ 29 K, whereas A_{AF1} increases monotonically with temperature. Such oscillatory components become 0 at T_N, while A_{tail} increases with further increasing temperature and approaches the maximum value above T_N.

As seen in Fig. 4(c), the relaxation rates, σ_{AF3} ranges below $10\,\mu s^{-1}$ and almost temperature independent up to about 25 K, i.e., in the vicinity of T_N. σ_{AF1}, on the other hand, poses $\sim 16\,\mu s^{-1}$ at the lowest temperature measured (2 K). At higher temperatures, it decreases with increasing temperature up to 22 K, and starts increasing again toward T_N like a critical behavior. On the contrary, $\sigma_{AF2} \sim 10\,\mu s^{-1}$ at 2 K and increases with temperature up to 20 K, then it decreases again and merges into σ_{AF3} at ~ 29 K.

For a field distribution at the muon site created by an IC magnetic structure, a cosine fit of the μ^+SR spectrum is known to provide a large delay of the initial phase (ϕ_{AF}) [19,20,37]. Indeed, both ϕ_{AF2} and ϕ_{AF3} range between -7 and $-50°$ even at 2 K due to the wide field distribution at the muon sites [Fig. 4(d)].

For the tail signal, which corresponds to the parallel component of the internal magnetic fields to the initial muon spin polarization, λ_{tail} is very small compared with λ_{AF} at temperatures below T_N, and decreases with decreasing temperature [Fig. 4(e)], as expected.

Overall, the μ^+SR parameters obtained by fitting with Eq. (1) vary continuously with temperature. However, as seen in Fig. 2(b), the Fourier transform spectrum at 2 K looks slightly different from those above 2 K. Such difference is explained by the increase in σ_{AF2} with temperature below 20 K, leading to a reduction of the height of the central peak
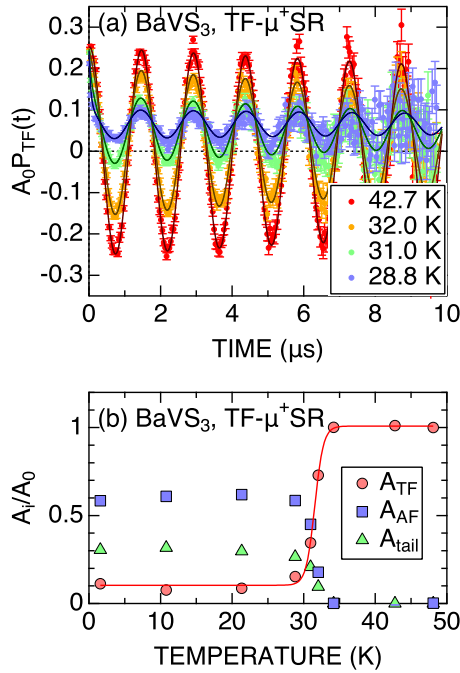
FIG. 6. (a) wTF-μ^+SR spectra for BaVS$_3$ recorded at selected temperatures and (b) the temperature dependencies of the three normalized asymmetries, A_{TF}/A_0, A_{AF}/A_0, and A_{tail}/A_0. The magnitude of wTF was 50 Oe. In (a), solid lines represent the best fits with Eq. (2). In (b), a solid line represents the best fit with a sigmoid function, and error bars are smaller than the data point symbols.

in Fig. 2(b) above 2 K. This also implies a small change in the field distribution formed by the IC-AF order, for the details are unknown at present. To clarify this, neutron diffraction work on a high-quality single-crystal sample is desirable, as already mentioned.

Finally, it should be noted that, besides the discrepancy between the estimated μ_{ord}^V from μ^+SR and neutron diffraction, the temperature dependencies of the μ^+SR parameters are consistent with the NMR [14,15] and neutron diffraction [16] results, i.e., the static AF order appears below $\sim$31 K.

B. wTF-μ^+SR at ambient pressure

Before the high-pressure μ^+SR measurements, μ^+SR spectra in wTF at selected temperature across the magnetic transition temperature were recorded [see Fig. 6(a)] to determine T_N. Here, weak means a very small field (50 Oe this time) compared with the internal AF field (H_{int}) and transverse represents the applied field direction that is perpendicular to the initial muon spin polarization. The muon spin precesses around wTF with a full asymmetry in a paramagnetic phase, but with zero asymmetry in a magnetically ordered phase when $H_{int} \gg$ wTF. In other words, the wTF asymmetry (A_{TF}) is roughly proportional to the volume fraction of the paramagnetic phases in the sample.

One can clearly observe in Fig 6(a) that, at 42.7 K, the spectrum exhibits a clear oscillation with a full asymmetry (0.25) and a very small damping, indicating that the whole volume of the BaVS$_3$ sample is in a paramagnetic state. As temperature decreases from 42.7 K, the asymmetry of the

oscillatory signal rapidly decreases, but a slowly relaxing background signal increases, which corresponds to the tail signal in the ZF spectrum. Hence, considering Eq. (1), the wTF-μ^+SR spectrum was fitted by a combination of an exponentially relaxing cosine oscillation due to wTF and two exponentially relaxing nonoscillatory signals caused by the AF oscillations and tail components,

$$A_0 P_{TF}(t) = A_{TF} \cos(2\pi f_{TF} t + \phi_{TF}) \exp(-\lambda_{TF} t)$$
$$+ A_{AF} \exp\left(-\frac{\sigma_{AF}^2 t^2}{2}\right)$$
$$+ A_{tail} \exp(-\lambda_{tail} t), \qquad (2)$$

where f_{TF} is the muon spin precession frequency due to wTF and is given by $f_{TF} = \gamma_\mu/2\pi \times 50\,\text{Oe} = 13.554\,\text{kHz/Oe} \times 50\,\text{Oe} \sim 0.68\,\text{MHz}$. The A_{AF} signal corresponds to the first three terms in Eq. (1), which are predominant in an early time domain below 0.5 μs. However, since we need to focus on the A_{TF} oscillatory signal up to 10 μs in the wTF-μ^+SR spectrum, the sum of the first three terms in Eq. (1) is simplified as one exponentially relaxing A_{AF} signal in Eq. (2).

Figure 6(b) shows the temperature dependencies of the three normalized asymmetries (A_i/A_0), where $A_0 = A_{TF}$ (48 K). As temperature decreases from 50 K, the $A_{TF}(T)/A_0$ curve exhibits a steplike decrease at around 30 K, while both A_{AF} and A_{tail} appear below 30 K. From the middle point of the steplike change in the $A_{TF}(T)/A_0$ curve, T_N is determined as 31.55(6) K. The fact that $A_{TF}/A_0 = 0.104(12)$ even below T_N indicates the presence of nonmagnetic impurity phases in the sample, but the volume fraction of such phases is about 10%.

C. wTF-μ^+SR at high pressures

Figure 7 shows the wTF-μ^+SR spectrum above and below T_N. Since the pressure cell is paramagnetic even at the lowest temperature achievable on the GPD, the muons stopped in the pressure cell provide (similar to a nonmagnetic impurity phase in the sample) an oscillatory signal due to wTF regardless of temperature. More correctly, a nonmagnetic impurity phase in the sample also provides a temperature-independent wTF oscillatory signal.

At temperatures above T_N, the muons stopped in the BaVS$_3$ phase also give an oscillatory signal due to wTF. The wTF-μ^+SR spectrum thus exhibits the wTF oscillation with a full asymmetry in total [Fig. 7(a)]. On the contrary, at temperatures below T_N, wTF in the BaVS$_3$ phase is hidden by the larger AF internal field, which is given by a sum of the AF oscillatory signals and 1/3 tail signal [Eq. (1)], leading to the loss of the wTF asymmetry from the BaVS$_3$ phase. In this case, about 40% of the implanted muons stop in the BaVS$_3$ phase and the rest 60% in the pressure cell [Fig. 7(b)] (more correctly, about 4% in the nonmagnetic impurity phase in the sample and 56% in the cell). Therefore, by measuring the wTF-μ^+SR spectrum as a function of temperature, T_N of BaVS$_3$ is clearly determined even in the pressure cell. The wTF-μ^+SR spectrum at high pressures was also fitted by Eq. (2).

Figure 8(a) shows the normalized $A_{TF}(T)$ [$A_{TF}(T)/A_0$] curves at several pressures. At ambient pressure, as T decreases from 45 K, the $A_{TF}(T)/A_0$ curve exhibits a sharp drop
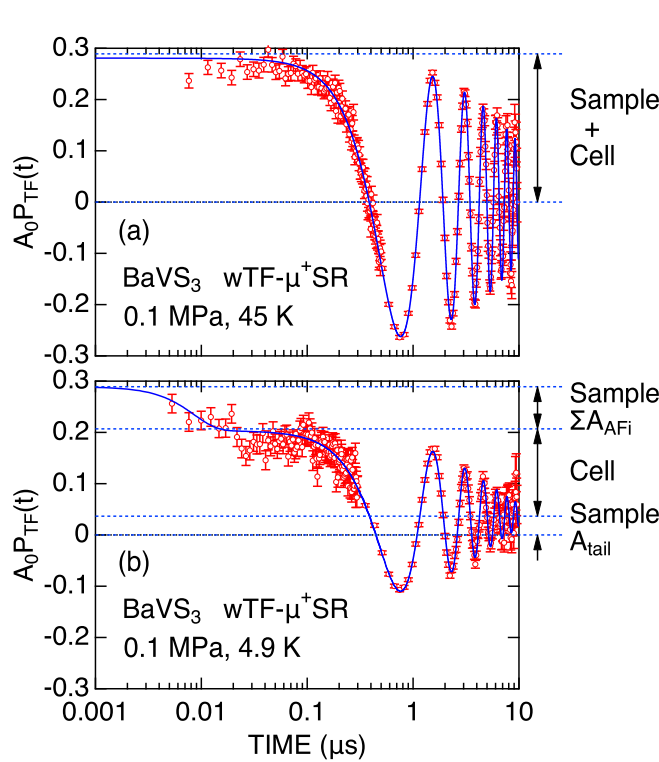
FIG. 7. The wTF-μ^+SR spectrum for the BaVS$_3$ sample in the pressure cell (a) above T_N (45.0 K) and (b) below T_N (4.9 K) at ambient pressure. The applied wTF was 50 Oe. In (a), both the sample and cell are paramagnetic, while in (b) only the cell is paramagnetic. From the wTF-μ^+SR spectrum in (b), the volume fraction of the cell is estimated as about 60%.

FIG. 8. (a) The temperature dependence of the normalized A_{TF} at several pressures and (b) the magnetic phase diagram determined with the wTF measurements. In (a), the data were obtained by fitting the wTF-μ^+SR spectrum with Eq. (2). In (b), blue solid and broken lines represent the structural phase boundaries determined with XRD, although the correct position of the broken line is ambiguous [11]. PM, PI/C, ICAFI/C, and ICAFI/IC represent paramagnetic metal, paramagnetic insulator with commensurate structure, incommensurate antiferromagnetic insulator with commensurate structure, and incommensurate antiferromagnetic insulator with incommensurate structure, respectively. Error bars are smaller than the data point symbol.

at 30 K, as in the case without pressure cell [Fig. 6(b)]. As mentioned above, since about 60% of the implanted muons stop in the pressure cell, which is paramagnetic even at the lowest temperature measured, A_{TF}/A_0 is ~0.6 below T_N [compare with Fig. 6(b) for the case without pressure cell]. From the middle point of the steplike change in the $A_{\mathrm{TF}}(T)/A_0$ curve, T_N is estimated as 30.2(3) K at ambient pressure, which is roughly equivalent to the value estimated from the wTF data obtained without pressure cell. The discrepancy between the GPD and GPS is probably caused by an indirect temperature measurement in the GPS, particularly for the fork-type folder, to which the sample is suspended by a Mylar tape. As pressure increases from ambient pressure, the transition temperature slightly shifts toward a lower temperature with pressure up to around 1.42 GPa. The transition temperature decreases rapidly at even higher pressures until finally it is completely suppressed at $p \geqslant 1.86$ GPa.

Using these $A_{\mathrm{TF}}(T)/A_0$ curves, the estimated T_N is plotted as a function of pressure together with the reported structural phase boundaries [11] in Fig. 8(b). T_N is almost pressure independent until the structural phase boundary at $p \sim 1.4 - 1.5$ GPa, suggesting that the magnetic phase boundary corresponds to the structural phase boundary at $p \geqslant 1.4$ GPa. Moreover, the magnetic order is completely suppressed at $p \geqslant 1.86$ GPa, where a high-pressure metallic phase is stabilized as a ground state. Therefore, among the proposed three
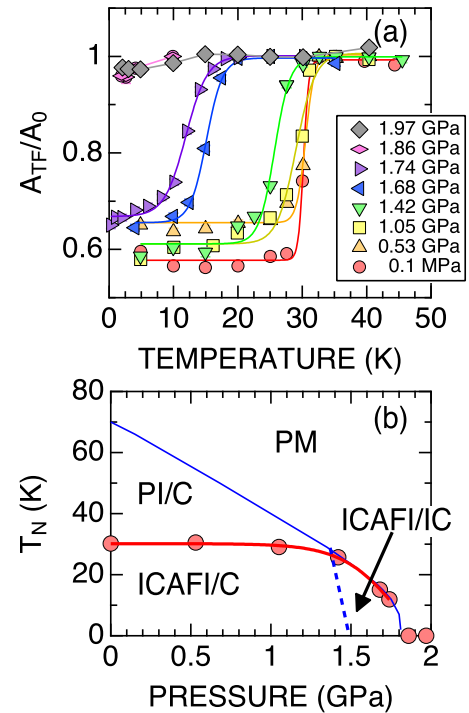
scenarios [17], the second one, in which T_N is suppressed to zero at $p = p_{\mathrm{cr}}$, is correct for BaVS$_3$.

The magnitude of A_{TF}/A_0 at the lowest temperature is found to slightly increase with pressure, meaning the decrease in the volume fraction of the sample with pressure. This is probably due to the compression of the pressed powder sample with pressure, which reduces the height of the sample discs and decreases the number of the muons stopped in the sample. Alternatively, the pressure medium, i.e., Daphne oil, could be compressed with pressure, leading to the increase in the density of the pressure medium. This would also reduce the number of the muons stopped in the sample. Since recent high-pressure μ^+SR measurements on K$_2$Cr$_8$O$_{16}$ using the same setup as this work also show a similar decrease in A_{TF}/A_0 with pressure [27], such decrease is most unlikely caused by an intrinsic change in the BaVS$_3$ sample.

D. ZF-μ^+SR at high pressures

To study the magnetic ground state at high pressures, the ZF-μ^+SR spectrum was also measured at the lowest temperature (see Fig. 9). It is very clear that the ZF-μ^+SR spectrum recorded at $p = 1.42$ and 1.68 GPa is essentially the same
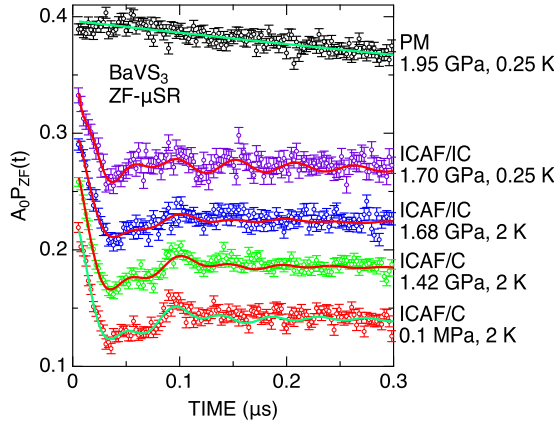
FIG. 9. The ZF-μ^+SR spectrum at the lowest temperature measured under five different pressures. Each spectrum is shifted upward by 0.03 for clarity of display.
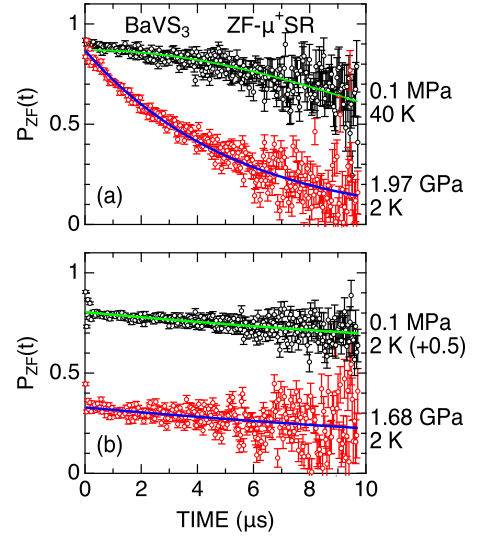

FIG. 10. Comparison of the two normalized ZF-μ^+SR spectra for BaVS₃ recorded in (a) the paramagnetic states and (b) the antiferromagnetic state. In (a), black symbol shows the spectrum at 0.1 MPa and 40 K, while red symbols shows that at 1.97 GPa and 2 K. In (b), black symbol shows the spectrum at 0.1 MPa and 2 K, while red symbols shows that at 1.68 GPa and 2 K. The spectra shown by red symbols were extracted from three ZF-μ^+SR spectra using Eq. (4). In (a), a green solid line represents the best fit using a Kubo-Toyabe function, while a blue solid line represents the best fit using an exponential relaxation function. In (b), solid lines represent the best fit using an exponential relaxation function.

as that recorded at ambient pressure, while the spectrum at $p = 1.74$ GPa is slightly different from those at $p \leqslant 1.68$ GPa. In the IC structure phase appearing in the high-p and low-T region, that is $p \geqslant 1.4$ GPa and $T \leqslant 30$ K [see Fig. 8(b)], the deviation from $1/2c^*$ is estimated as 0.015–0.024, whereas no change in a^* and b^* was observed [11]. Such a small structural modification along the c axis is unlikely to drastically alter the internal magnetic field caused by the IC-AF order in the ab plane, because the intrachain 1D interaction along the c axis is FM. This is consistent with the ZF-μ^+SR result. On the other hand, the ZF-μ^+SR confirms the absence of magnetic order down to 0.25 K, when $p = 1.95$ GPa.

In the BaVS₃ lattice, the intrachain 1D FM interaction is known to be stronger than the interchain 2D AF interaction [7]. This could raise a question on the presence of a phase formed by either long or short FM-ordered 1D chains without the 2D-AF order at high pressures, i.e., such a FM-ordered 1D chain behaves as a localized moment [22]. However, the ZF-μ^+SR spectrum recorded at $T = 0.25$ K with $p = 1.95$ GPa demonstrates the absence of magnetic order. This suggests that both 1D-FM and 2D-AF interactions are suppressed by pressure, particularly at $p > 1.4$ GPa, and any magnetic order entirely vanishes at $p \geqslant p_{cr}$. Therefore, we can exclude a contribution of magnetic order to the origin of a non-Fermi-liquid behavior observed by resistivity measurements at $p > p_{cr}$ and $T < 40$ K [9].

To obtain H_{int} in BaVS₃ at high pressures, we have attempted to extract the ZF-μ^+SR spectrum for BaVS₃, particularly in a slow time domain, from the spectrum recorded using a pressure cell. Such a spectrum is naturally represented as

$$A_0 P_{ZF}(p, T, t) = A_C P_{ZF,C}(p, T, t) + A_S P_{ZF,S}(p, T, t), \quad (3)$$

where A_C and A_S are the asymmetries from the pressure cell and sample, and $P_{ZF,C}(p, T, t)$ and $P_{ZF,S}(p, T, t)$ are their respective depolarization function. $P_{ZF,C}(p, T, t)$ is known to be almost independent of p and T above 1.5 K [26]. Thus, if we ignore the small variations in A_C and A_S with p, $P_{ZF,S}(p, T, t)$

is roughly given by

$$A_S P_{ZF,S}(p, T, t) = A_0 P_{ZF}(p, T, t) - A_0 P_{ZF}(0.1 \text{MPa}, T, t)$$
$$+ A_S P_{ZF,S}(0.1 \text{MPa}, T, t). \quad (4)$$

The ZF-μ^+SR measurements without pressure cell provide information about $P_{ZF,S}(0.1 \text{MPa}, T, t)$ and $A_S \sim 0.42$ ($A_C \sim 0.58$) is obtained from Fig. 8(a). As a result, $P_{ZF,S}(p, T, t)$ at $p = 1.97$ GPa and $T = 2$ K is estimated as shown in Fig. 10(a), in which $P_{ZF,S}(0.1 \text{MPa}, T, t)$ at $T = 40$ K is also plotted for comparison. Considering the fact that $A_{BG}/A_0 = 0.1$ from the wTF measurements without pressure cell [see Fig. 6(b)], the maximum value of P_{ZF} for the BaVS₃ phase is fixed at 0.9.

In the paramagnetic state at $p = 0.1$ MPa and $T = 40$ K, the ZF-μ^+SR spectrum is fitted by a static Kubo-Toyabe function, $\frac{1}{3} + \frac{2}{3}(1 - \Delta^2 t^2) \exp(-\frac{\Delta^2 t^2}{2})$, with the field distribution width $\Delta = 0.060(2)\ \mu s^{-1}$ [corresponding to 0.70(2) Oe], which indicates that each muon *feels* only a nuclear magnetic field, i.e., the absence of localized V moments above T_N. On the other hand, in the pressure induced paramagnetic state at $p = 1.97$ GPa and $T = 2$ K, the time spectrum is fitted by an exponential relaxation function, $\exp(-\lambda t)$, with $\lambda = 0.185(6)\ \mu s^{-1}$. This means that a slowly fluctuating H_{int} caused by V moments are present even in a metallic state. Such slowly fluctuating H_{int} is most likely the origin of a non-Fermi-liquid behavior [9] around QCT.

To demonstrate the reliability of such extracted spectrum, Fig. 10(b) shows the comparison of the two normalized ZF-μ^+SR spectra in the AF state; that is, $P_{ZF,S}(p, T, t)$ at

$p = 1.68$ GPa and $T = 2$ K and $P_{ZF,S}(0.1 MPa, T, t)$ at $T = 2$ K, which was recorded without pressure cell. Besides the oscillatory signal in an early time domain, both spectra exhibit the $1/3$ tail signal in the AF ordered state. A fit using an exponential relaxation function, $(A_{tail}/A_0) \exp(-\lambda_{tail} t)$, in the time domain between 0.5 and 9.7 μs provides that $(A_{tail}/A_0) = 0.329(12)$ and $\lambda_{tail} = 0.038(7) \mu s^{-1}$ for the time spectrum under pressure, while $(A_{tail}/A_0) = 0.304(6)$ and $\lambda_{tail} = 0.044(4) \mu s^{-1}$ for the time spectrum at ambient pressure. Considering the small variations in A_C and A_S with p, such extraction is found to give a reasonable ZF-μ^+SR spectrum for the sample in a pressure cell.

IV. SUMMARY

We have investigated the microscopic magnetic nature of BaVS$_3$ at ambient and high pressures with μ^+SR using a powder sample. The μ^+SR measurements in a zero magnetic field (ZF) at ambient pressure clarified the appearance of a clear oscillatory signal below $T_N = 31$ K, which evidenced the formation of static AF order. The analysis of an internal magnetic field supported an incommensurate linear spin density wave order as a magnetic ground state of BaVS$_3$.

The μ^+SR measurements in a wTF at high pressures showed that T_N is almost pressure (p) independent up to 1.4 GPa, then T_N decreases rapidly with p for $p > 1.4$ GPa and finally disappears at $p_{cr} \sim 1.8$ GPa, above which a paramagnetic phase is stabilized. This suggested that the AF order is coupled with a metal-insulator transition caused by the formation of long-range structural order. According to the ZF-μ^+SR measurements at the lowest temperature measured, it was found that the internal AF field is almost p independent up to p_{cr} and vanishes above p_{cr}, but a slowly fluctuating internal magnetic field appears instead.

APPENDIX

The magnetic properties of BaVS$_3$ are known to be sensitive to sulfur deficiency, which induces FM order below about $T_C \leqslant 15$ K [4,42–45]. To study the effect of sulfur deficiency on the local magnetic environments, we have also
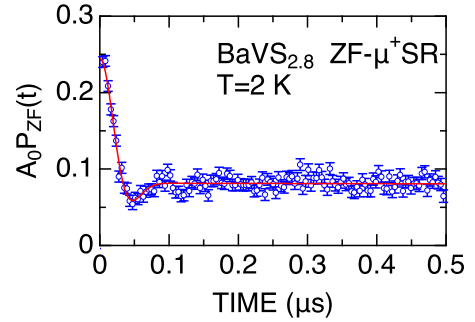

FIG. 11. The ZF-μ^+SR time spectrum for BaVS$_{2.8}$ recorded at 2 K. A solid line represents a best fit with Eq. (A1).

measured the μ^+SR spectrum for BaVS$_{2.8}$ at 0.1 MPa and 2.44 GPa. The BaVS$_{2.8}$ sample was prepared by a solid-state reaction technique between BaS, V, and S, as well as BaVS$_3$, but without postheating with S [5,44]. Note that the amount of S is a nominal composition. Figure 11 shows the ZF-μ^+SR time spectrum recorded at 2 K without pressure cell, i.e., at 0.1 MPa. The ZF-μ^+SR spectrum is found to exhibit a strongly damped oscillation compared with that of BaVS$_3$ [see Fig. 2(a)]. Such spectrum is reasonably fitted with [33]

$$A_0 P_{ZF}(t) = A_1 \cos(2\pi f_1 t) \exp\left(-\frac{\sigma^2 t^2}{2}\right)$$
$$+ \frac{1}{2} A_1 \exp(-\lambda t). \quad (A1)$$

The fit provided with $A_1 = 0.1631(10)$, $f_1 = 7.4(2)$ MHz, which roughly corresponds to $H_{int} = 550(13)$ Oe, and $\sigma = 36.1(1.3) \mu s^{-1}$, $\lambda = 0.021(2) \mu s^{-1}$, and $\gamma_\mu^{-1}\sqrt{\omega^2 + \sigma^2} = 693(20)$ Oe, where $\omega = 2\pi f_1$.

Figure 12 shows the temperature dependencies of the normalized wTF asymmetry (A_{TF}/A_0) for the BaVS$_{2.8}$ sample in the pressure cell recorded at 0.1 MPa and 2.44 GPa. Since the $A_{TF}(T)/A_0$ curve at 0.1 MPa shows two steplike changes at 29.98(2) K and 13.92(2) K, the BaVS$_{2.8}$ sample is found to consist of two phases. Namely, one is the BaVS$_3$ phase with $T_N \sim 30$ K and the other is the BaVS$_{3-\delta}$ phase with
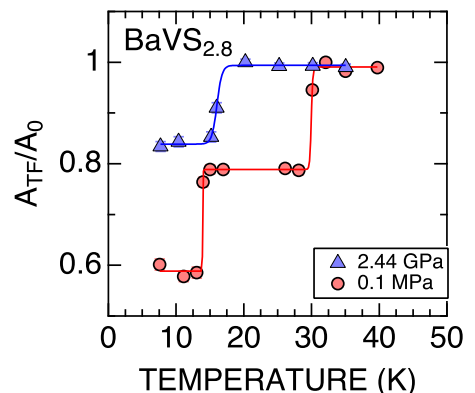

FIG. 12. The temperature dependence of the normalized A_{TF} for the BaVS$_{2.8}$ sample in the pressure cell recorded at 0.1 MPa and 2.44 GPa.

$T_C \sim 14$ K. The volume fraction of each phase is about 50%. The wTF measurements without pressure cell also supported above estimations.

On the contrary, the $A_{TF}(T)/A_0$ curve at 2.44 GPa exhibits one steplike change at $T_C = 16.04(6)$ K, revealing that the $BaVS_{3-\delta}$ phase is still in a FM state. This is because $BaVS_3$ enters into a paramagnetic phase above 1.8 GPa (see Fig. 8). Furthermore, since T_C is slightly increasing with p, the $BaVS_{3-\delta}$ phase with $T_C \sim 14$ K does not correspond to the focused material in this paper. This also demonstrates the importance of stoichiometry in the $BaVS_3$ sample for clarifying the magnetic nature.

---

[1] M. Imada, A. Fujimori, and Y. Tokura, Rev. Mod. Phys. **70**, 1039 (1998).

[2] R. A. Gardner, M. Vlasse, and A. Wold, Acta Crystallogr. Sec. B **25**, 781 (1969).

[3] M. Takano, H. Kosugi, N. Nakanishi, M. Shimada, T. Wada, and M. Koizumi, J. Phys. Soc. Jpn. **43**, 1101 (1977).

[4] O. Massenet, J. Since, J. Mercier, M. Avignon, R. Buder, V. Nguyen, and J. Kelber, J. Phys. Chem. Solids **40**, 573 (1979).

[5] H. Imai, H. Wada, and M. Shiga, J. Phys. Soc. Jpn. **65**, 3460 (1996).

[6] T. Inami, K. Ohwada, H. Kimura, M. Watanabe, Y. Noda, H. Nakamura, T. Yamasaki, M. Shiga, N. Ikeda, and Y. Murakami, Phys. Rev. B **66**, 073108 (2002).

[7] X. Jiang and G. Y. Guo, Phys. Rev. B **70**, 035110 (2004).

[8] T. Graf, D. Mandrus, J. M. Lawrence, J. D. Thompson, P. C. Canfield, S.-W. Cheong, and L. W. Rupp, Phys. Rev. B **51**, 2037 (1995).

[9] L. Forró, R. Gaál, H. Berger, P. Fazekas, K. Penc, I. Kézsmárki, and G. Mihály, Phys. Rev. Lett. **85**, 1938 (2000).

[10] I. Kézsmárki, G. Mihály, R. Gaál, N. Barišić, H. Berger, L. Forró, C. C. Homes, and L. Mihály, Phys. Rev. B **71**, 193103 (2005).

[11] S. Bernu, P. Fertey, J.-P. Itié, H. Berger, P. Foury-Leylekian, and J.-P. Pouget, Phys. Rev. B **86**, 235105 (2012).

[12] K. Penc, M. Mambrini, P. Fazekas, and F. Mila, Phys. Rev. B **68**, 012408 (2003).

[13] K. Momma and F. Izumi, J. Appl. Cryst. **44**, 1272 (2011).

[14] H. Nishihara and M. Takano, J. Phys. Soc. Jpn. **50**, 426 (1981).

[15] H. Nakamura, H. Imai, and M. Shiga, Phys. Rev. Lett. **79**, 3779 (1997).

[16] H. Nakamura, T. Yamasaki, S. Giri, H. Imai, M. Shiga, K. Kojima, M. Nishi, K. Kakurai, and N. Metoki, J. Phys. Soc. Jpn. **69**, 2763 (2000).

[17] P. Fazekas, K. Penc, K. Radnoczi, N. Barišić, H. Berger, L. Forró, S. Mitrović, A. Gauzzi, L. Demkó, I. Kézsmárki et al., J. Magn. Magn. Mater. **310**, 928 (2007).

[18] P. Fazekas, N. Barišić, I. Kézsmárki, L. Demkó, H. Berger, L. Forró, and G. Mihály, Phys. Rev. B **75**, 035128 (2007).

[19] G. M. Kalvius, D. R. Noakes, and O. Hartmann, Handbook on the Physics and Chemistry of Rare Earths (North-Holland, Amsterdam, 2001), Vol. 32, Chap. 206, pp. 55–451.

[20] A. Yaouanc and P. Dde Réotier, Muon Spin Rotation, Relaxation, and Resonance, Application to Condensed Matter (Oxford, New York, 2011).

[21] J. Sugiyama, H. Nozaki, J. H. Brewer, E. J. Ansaldo, T. Takami, H. Ikuta, and U. Mizutani, Phys. Rev. B **72**, 064418 (2005).

[22] J. Sugiyama, H. Nozaki, Y. Ikeda, K. Mukai, D. Andreica, A. Amato, J. H. Brewer, E. J. Ansaldo, G. D. Morris, T. Takami et al., Phys. Rev. Lett. **96**, 197206 (2006).

[23] H. Nozaki, M. Janoschek, B. Roessli, J. Sugiyama, L. Keller, J. H. Brewer, E. J. Ansaldo, G. D. Morris, T. Takami, and H. Ikuta, Phys. Rev. B **76**, 014402 (2007).

[24] J. Sugiyama, H. Nozaki, Y. Ikeda, P. L. Russo, K. Mukai, D. Andreica, A. Amato, T. Takami, and H. Ikuta, Phys. Rev. B **77**, 092409 (2008).

[25] Z. Shermadini, R. Khasanov, M. Elender, G. Simutis, Z. Guguchia, K. Kamenev, and A. Amato, High Pressure Res. **37**, 449 (2017).

[26] R. Khasanov, Z. Guguchia, A. Maisuradze, D. Andreica, M. Elender, A. Raselli, Z. Shermadini, T. Goko, F. Knecht, E. Morenzoni et al., High Pressure Res. **36**, 140 (2016).

[27] O. K. Forslund, D. Andreica, Y. Sassa, H. Nozaki, I. Umegaki, E. Nocerino, V. Jonsson, O. Tjernberg, Z. Guguchia, Z. Shermadini et al., Sci. Rep. **9**, 1141 (2019).

[28] A. Suter and B. Wojek, Phys. Procedia **30**, 69 (2012).

[29] G. Kresse and J. Hafner, Phys. Rev. B **47**, 558 (1993).

[30] F. L. Pratt, Dipolar Field Calculations for Muon Spectroscopy (2019), https://doi.org/10.5281/zenodo.3476167.

[31] P. Leininger, V. Ilakovac, Y. Joly, E. Schierle, E. Weschke, O. Bunau, H. Berger, J.-P. Pouget, and P. Foury-Leylekian, Phys. Rev. Lett. **106**, 167203 (2011).

[32] W. Higemoto, A. Koda, G. Maruta, K. Nishiyama, H. Nakamura, S. Giri, and M. Shiga, J. Phys. Soc. Jpn. **71**, 2361 (2002).

[33] G. Allodi, A. Prodi, R. D. Renzi, F. Licci, F. Bolzoni, G. Guidi, E. Gilioli, A. Gauzzi, M. Marezio, and R. Scheuermann, Physica B: Cond. Matter **374-375**, 44 (2006).

[34] R. A. de Souza, U. Staub, V. Scagnoli, M. Garganourakis, Y. Bodenthin, and H. Berger, Phys. Rev. B **84**, 014409 (2011).

[35] O. Ofer, Y. Ikedo, T. Goko, M. Månsson, J. Sugiyama, E. J. Ansaldo, J. H. Brewer, K. H. Chow, and H. Sakurai, Phys. Rev. B **82**, 094410 (2010).

[36] J. Sugiyama, K. Mukai, H. Nozaki, M. Harada, M. Månsson, K. Kamazawa, D. Andreica, A. Amato, and A. D. Hillier, Phys. Rev. B **87**, 024409 (2013).

[37] D. Andreica, Ph.D. thesis, ETH Zurich, 2001.

[38] J. F. Herbst, J. J. Croat, F. E. Pinkerton, and W. B. Yelon, Phys. Rev. B **29**, 4176 (1984).

[39] A. Teplykh, Y. Chukalkin, S. Lee, S. Bogdanov, N. Kudrevatykh, E. Rosenfeld, Y. Skryabin, Y. Choi, A. Andreev, and A. Pirogov, J. Alloys Compd. **581**, 423 (2013).

[40] P. Wolfers, S. Obbade, D. Fruchart, and R. Verhoef, J. Alloys Compd. **242**, 74 (1996).

[41] J. Sugiyama, K. Miwa, H. Nozaki, Y. Kaneko, B. Hitti, D. Arseneau, G. D. Morris, E. J. Ansaldo, and J. H. Brewer, Phys. Rev. Mater. **3**, 064402 (2019).

[42] O. Massenet, R. Buder, J. Since, C. Schlenker, J. Mercier, J. Kelber, and D. Stucky, Mater. Res. Bull. **13**, 187 (1978).

[43] J. Kelber, A. Aldred, G. Lander, M. Mueller, O. Massenet, and G. Stucky, J. Solid State Chem. **32**, 351 (1980).

[44] T. Yamasaki, H. Nakamura, and M. Shiga, J. Phys. Soc. Jpn. **69**, 3068 (2000).

[45] P. Foury-Leylekian, P. Leininger, V. Ilakovac, Y. Joly, S. Bernu, S. Fagot, and J.-P. Pouget, Physica B: Cond. Matter **407**, 1692 (2012).